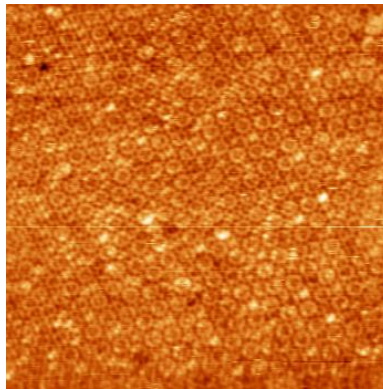


Quasicrystals (need a title)

M. Darlington

April 29, 2008



Abstract

This project is on the characterisation of the fivefold surface of *i*-Ag-Yb-In using STM and LEED. It includes; step and terrace morphology; step height distribution; using high resolution imaging to deduce a Yb rich surface and finding the magnitude of the reciprocal lattice vector. In addition to this it gives a brief introduction to the theory behind quasicrystals and covers surface science techniques extensively

Contents

1	Introduction	4
2	Quasicrystals	6
3	Tiling and Crystallography	9
3.1	Crystals and Crystallography	11
3.2	Aperiodic Order	13
3.3	Penrose Tiling	16
4	Types of Quasicrystal	17
4.1	Icosahedral Quasicrystal	17
4.2	Decagonal Quasicrystal	18
5	Equipment and procedures	20
5.1	Under my Little Fingernail	20
5.2	Creating a Vacuum	22
5.3	LEED	26
5.4	STM	28
5.5	Ion Sputtering	29
5.6	Annealling	30
5.7	Diamond Paste Polishing	30
6	Experiments	30
6.1	Step Morphology	30
6.2	Terrace Morphology	33
6.3	Step Height Distribution	34
6.4	High Resolution Image	35
6.5	LEED - Long Range Order	40
6.6	Different Domains in the Sample	42

6.7 Pb and C60 Deposition	43
7 Conclusion	45

1 Introduction

This project begins with a brief introduction to quasicrystals which is required as they are different from any other material; this is covered in section 2. Having only been first discovered two decades ago, new varieties have been produced and continue to be found. One such quasicrystal is *i*-Ag-Yb-In and it is this around which I have based my project. It is unique because it shares its structure with binary *i*-Cd-In whereas all other quasicrystals stable under vacuum are tertiary; this is covered in more depth in section 4.1. The possible uses for quasicrystals is extensive as their properties include; low friction coefficients; “non stick” properties; more stable catalysts at high temperature and even hydrogen storage

Section 3.1 gives a short background in tilings and crystallography, concentrating on highlighting why quasicrystals are different to normal crystals with respect to their forbidden fivefold and tenfold symmetries. Quasicrystals are based around an ordered yet aperiodic structure known as a penrose tiling which allow them to have their forbidden symmetries. This is covered in sections 3.2 and 3.3.

Section 4 covers the two main types of quasicrystal, icosahedral and decagonal. *i*-Ag-Yb-In is an icosahedral quasicrystal which means it is quasicrystalline in three dimensions. Decagonal quasicrystals are two dimensional quasicrystals which are layered periodically.

By using STM it was possible to gather data on step and terrace morphology which is covered in section 6.1 and 6.2 respectively. Also by STM the step height distribution (section 6.3) was found to be; $S \rightarrow 0.28 \pm 0.04\text{nm}$; probability = $64 \pm 8\%$; $L \rightarrow 0.57 \pm 0.03\text{nm}$; probability = $9 \pm 3\%$ and $S+L \rightarrow 0.86 \pm 0.03\text{nm}$; probability = $15 \pm 4\%$. By taking a high resolution image and

comparing to a model, it was found that the surfaces of the terraces are probably constructed out of Yb (section 6.4). From LEED the magnitude of the reciprocal lattice vector was found to be 0.51 \AA^{-1} (section 6.5).

During the main experiments it was found that the sample was not uniform and contained two quasicrystal domains at different orientations (section 6.6). After the main experiments were finished we went on to coat the surface in Pb and found that it forms a quasicrystalline monolayer (section 6.7).

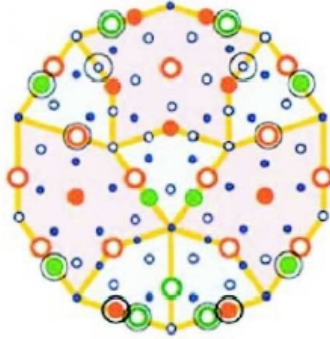


Figure 1: An example of a theoretical decagonal Al-Ni-Co cluster [2]

2 Quasicrystals

This final project was based around quasicrystals, specifically a new type of quasicrystal made from an alloy of silver rather than an alloy of aluminium. At the time which this article was written, silver based quasicrystals are more rare than diamond.

Quasicrystals were first discovered around two decades ago during a TEM experiment and have since been recognised as a new form of solid matter [7]. They are different from crystals in that they have no periodicity however, they do have long range order [1]. This order is seen in the results of a LEED experiment where rotational symmetries are seen. The rotational symmetries are usually 5-fold or 10-fold both of which are forbidden by the laws of crystallography[1]. At the time of their discovery these laws were thought unbreakable and quasicrystals were dismissed as a mistake but soon experimental evidence outweighed any doubt.

Quasicrystals consist of clusters of atoms arranged in pattern which is individual to each type of quasicrystal. Between these clusters are “glue”



Figure 2: Cybernox cooking set, coated with a quasicrystal non-stick layer [4]

atoms [1]. So far quasicrystals have always been a metal alloy and most of the ones which are stable under vacuum are aluminum based though the composition, shapes of clusters and symmetry axis can vary [3]. All natural quasicrystals discovered so far have an exotic composition of metals, most commonly consisting of three elements [3].

Quasicrystals have many unusual properties which have already been spotted by industry and I will mention some here. They have very low friction coefficients and “non stick” properties [3] which have already been used in the form of a frying pan [4]. In this form it has the advantage over Teflon in its hard enough to survive metal cooking implements however, it has the disadvantage in the enormous difference in price.

As mentioned, quasicrystals are more durable than Teflon. In fact they are very hard and their use in hard coatings has been recognised [3]. A more hypothetical use has been suggested, hydrogen storage in which the explosive gas is safely contained until needed. This reduces the risk of unwanted explo-

sions. Added to this their use as catalysts which show higher reactivity and more thermal stability than their normal metal counterparts [5]. Quasicrystals are very useful indeed.

There is a major problem; the exotic composition of quasicrystals are extremely hard to make. This makes them expensive and unprofitable which is bad for businesses trying to make a profit from them. Finding out why quasicrystals have such properties could, in the future, lead us to a cheaper way of production. That main question that needs answering is do the properties come from the structure or the chemical composition? The best way of answering this would be to produce a single element quasicrystal and test its properties in comparison to its natural structure. A promising way of doing this is to deposit a single element thin film on a quasicrystal surface where, in some cases, it takes on the same structure as the quasicrystal for one monolayer [6]. With the correct combination of quasicrystal and deposition element this could be improved. The final aim would be to produce a crystal of single element quasicrystal. If this were to have the same properties of natural" quasicrystals it would be a breakthrough but this is a long way off.

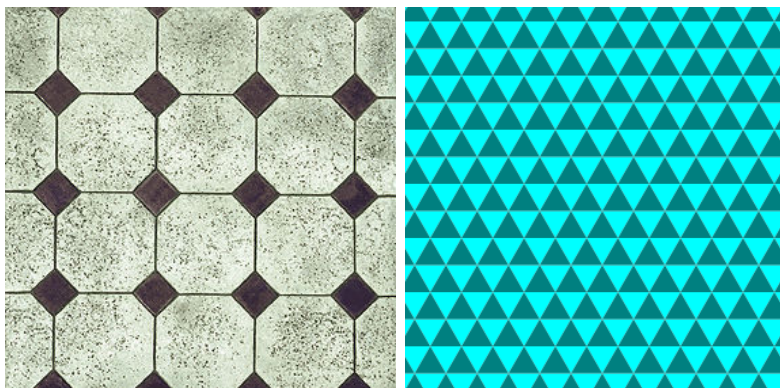


Figure 3: Left: Example of an octagon and square based tiling with four-fold rotational symmetry. Right: Example of a triangle based tiling with a threefold rotational symmetry.

3 Tiling and Crystallography

Tiling was invented long before the idea of the atom, yet is still very important in surface science. With tiling the most important concept is that of filling the space with shapes, leaving no gaps. This can be done in many ways however let us impose a rule. A line must be able to connect any vertex to any other vertex without leaving the shape, this is known as a concave shape. This drastically reduces the amount of shapes available to tile with.

Another important concept is rotational symmetry. This can be thought of as taking the tiling and rotating through one full rotation and counting how many times the original pattern appears. For example, a tiling of triangles would repeat three times whereas a tiling of octagons and squares (squares are required to fill the gaps) repeats four times. This is known respectively as 3-fold and 4-fold rotational symmetry. After many years of experimenting with tilings mathematicians found that they could only have 2, 3, 4, and 6-fold rotational symmetry. This can be seen when trying to slot together basic

polygons with the same rotational symmetry. A bright mathematician, Sir Roger Penrose, had occasionally dabbled in creating lattices with forbidden rotational symmetry but this was more of a hobby than an actual prediction.

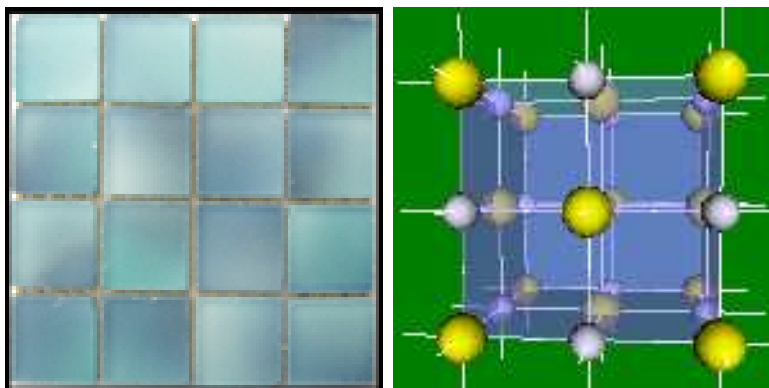


Figure 4: Left: Square stone tiles. Right: Model of an NaCl crystal showing the square tiling pattern in the planes.

3.1 Crystals and Crystallography

Why is it important to go into so much detail over a skill used to tile bathroom floors? Most normal solid matter is crystalline and therefore made from planes of atoms stacked on top of each other without any gaps (ideally). Another property of crystalline solids is that in any plane they must have a repeating pattern of atoms. If the atoms are considered vertices of polygons it can now be seen that the atomic planes are comparable to a tiling if all the polygons are isohedral. With this revelation we can now use our age old knowledge of tiling to make predictions of structures on the atomic level.

There are a finite number of tilings which are made from isohedral shapes, these are known as Laves nets and there are only eleven of them. This allows us to make the prediction that there are only eleven ways in which the atoms in a plane can be arranged and gives us a great way of categorising planes. However, as with many things it is not that simple. So far this project has assumed that the atoms making the crystal are all of the same type and this is not always the case. This leads to the idea of a basis where we assign a

group of atoms to each lattice point.

By using diffraction we can find the rotational symmetry and lattice vectors of a crystal. This is covered in more detail in section 4.3 where I discuss using LEED, however it is worth mentioning that diffraction can also be performed using X-rays.

3.2 Aperiodic Order

How can something be both aperiodic and ordered at the same time? Aperiodic could be used to describe a sequence that never repeats yet this does not have to be ordered. If this sequence still has rules which were used to create it, this is what brings order to the system. A famous example of this type of aperiodic order is the Fibonacci sequence where the rule to create it is the next term in the sequence is the sum of the two previous terms. Starting from one this continues as: 1, 1, 2, 3, 5, 8, 13, 21, 34

The Fibonacci sequence can be rewritten using the symbols S and L. If we use the rules S goes to L and L goes to LS and starting from S gives:

S
L
LS
LSL
LSLLS
LSLLSLSL
LSLLSLSLLSLLS

This sequence does not stop growing, yet no matter how large it gets it never repeats itself. The ratio of Ss to Ls gives the golden ratio which is well known to artists and architects. The Fibonacci Number is $\frac{1 + \sqrt{5}}{2}$

This sequence can be generated in a different way. Starting with a two dimensional square lattice, a line is drawn from $[0, 0]$ (or any integer coordinates). The line is at an irrational angle and will therefore never directly intercept an integer coordinate apart from the original set. By taking a second line parallel to the first at a distance relating to the angle we can create

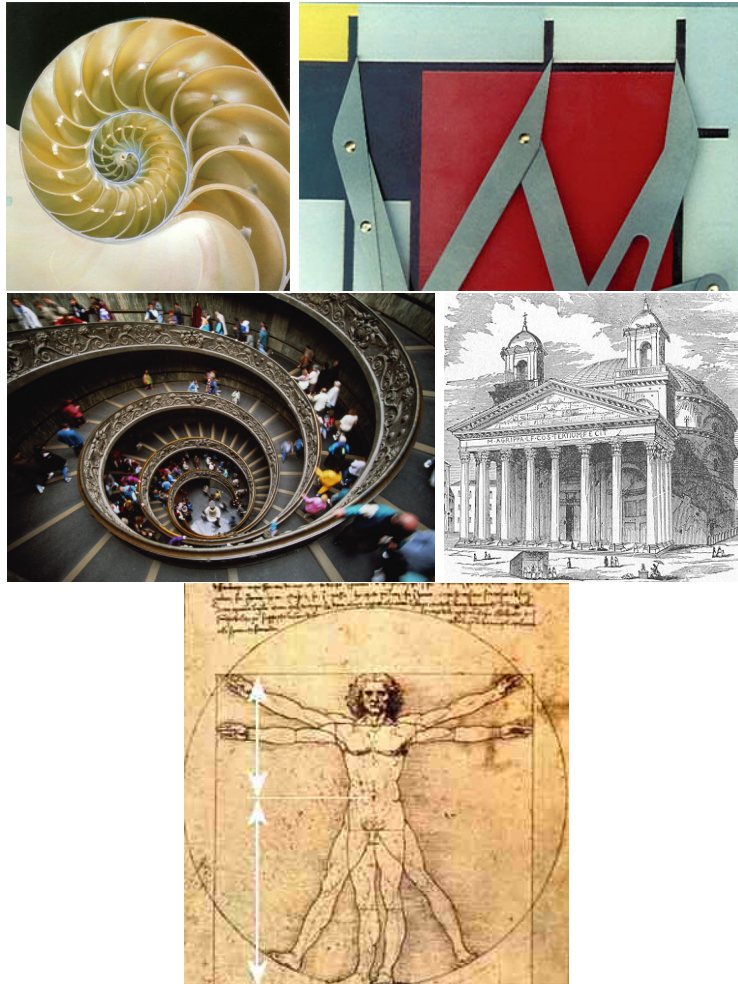


Figure 5: Top Left: A shell, the factor of the difference in width after each rotation is the golden ratio. Top left is the composition in red yellow and blue by Mondrian which is composed using the golden ratio. Middle left: As with the shell, this spiral staircase is constructed so it looks like the width increases each time by a factor equivalent to the golden ratio. Middle right: The Pantheon of ancient Rome was constructed using the golden ratio. Bottom: Da Vinci's Vitruvian Man is based around the golden ratio.

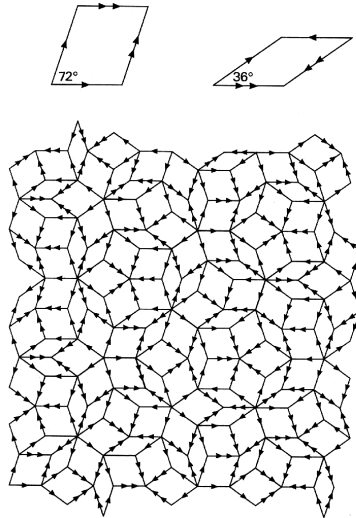


Figure 7: P1 Penrose tiling with matching rules

3.3 Penrose Tiling

Penrose tilings were created by ** Penrose as a way to fill a plane or space with a pattern giving forbidden rotational symmetries. He knew this could not be done with a single shape and instead used a small finite number of shapes or polygons. These shapes have to be put together with certain rules thus generating order and the rotational symmetry. At the same time these patterns must also be aperiodic. This is a much simpler way of modeling an aperiodic 2D or 3D lattice than the method above as the vectors of the Penrose tiling give you the lattice points. The easiest 2D Penrose tiling to draw is the P1 tiling. It is constructed from two types of Rhombuses with set angles of 108° and 72° for one and 144° and 36° for the other. These must be placed so the arrows match up. This is what gives us order.

By filling a space with the rhombohedrons a 3D penrose tiling can be constructed in a similar way. The vertices of this tiling is a 3D quasicrystalline structure.

4 Types of Quasicrystal

4.1 Icosahedral Quasicrystal

Icosahedral quasicrystals are aperiodic in all three dimensions. The rotational symmetry they exhibit depends on the direction at which you look at the sample. They have ten 3 fold axes, six fivefold axes and fifteen twofold axes. This is like an icosahedron. The structure of the icosahedral quasicrystal follows a 3D Penrose tiling giving a 3D quasicrystal. Clusters are positioned on the vertices of this tiling. (picture of cluster) Icosahedral quasicrystals are usually denoted by an italic *i*- before the chemical composition. Examples of icosahedral quasicrystals are *i*-Cd₈₄-Yb₁₆ (here after *i*-Cd-Yb, *i*-Ag₄₂-Yb₄₂-In₁₆ (here after *i*-Ag-Yb-In) and *i*-Al-Pd-Mg [3]. *i*-CdYb and *i*-AgYbIn are the two most important quasicrystals for this project. *i*-CdYb is a binary quasicrystal as it consists of only two elements, however it cannot survive under UHV as the Cd vapourises. To try and compensate for this The Cd was removed and replaced with a equal ammounts of Ag and In. By attempting to classify and understand the *i*-AgYbIn quasicrystal we can try to prove that it has the same binary structure as i-CdYb. If it does then we can go on to discover if binary systems have different properties to three element quasicrystals.

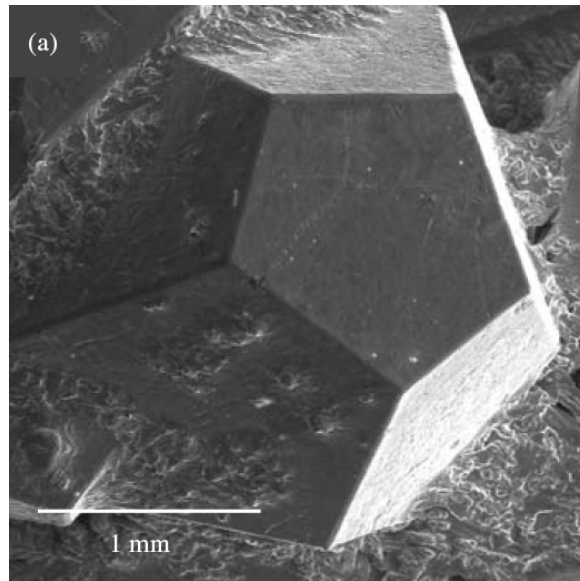


Figure 8: SEM micrograph showing *i*-Al-Pd-Re [9]

4.2 Decagonal Quasicrystal

Decagonal quasicrystals do not feature in this project but are worth mentioning as they are the other common type of quasi crystals. They are again constructed out of a Penrose tiling but they are only quasicrystalline in two dimensions. The quasicrystalline layers are stacked on top of each other periodically.

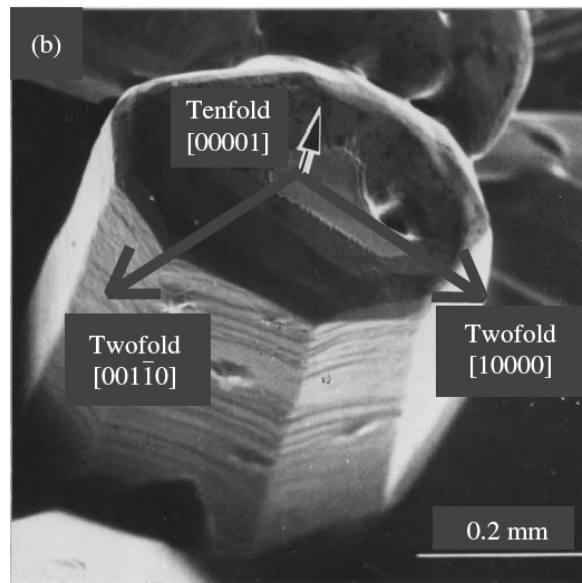


Figure 9: SEM micrograph showing *d*-Al-Ni-Co and its high symmetry axes [10]

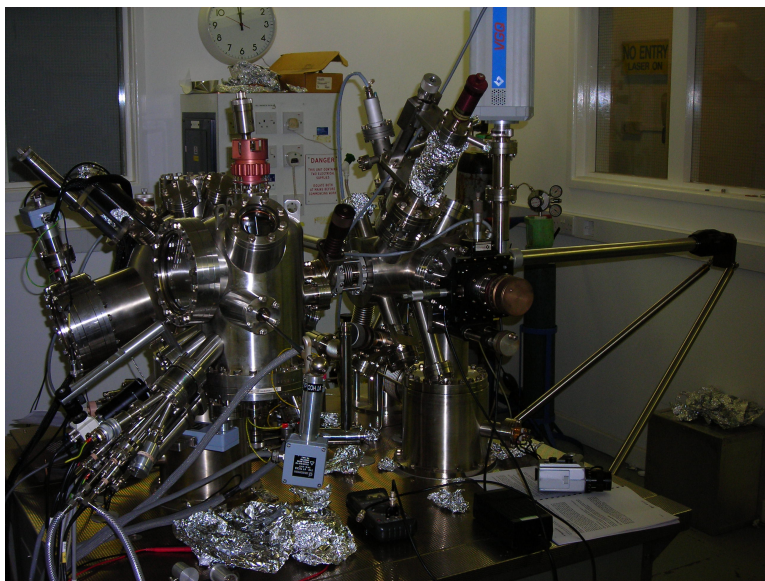


Figure 10: Variable temperature STM and LEED

5 Equipment and procedures

Many different techniques are used in surface science so this project will only discuss those which were used in my project. The important techniques were; creating the UHV environment; preparing the sample surface and taking measurements.

5.1 Under my Little Fingernail

An Ultra High Vacuum environment is necessary for experiments in surface science because it allows us to maintain a clean surface for an extended period of time. A surface becomes unusable when atoms from the environment bombard it and bind to form a monolayer. If we look at where pressure comes from we can see why it is such an important measurement. Pressure is the force per unit area the atoms in the environment exert when hitting a surface.

There are only two variables for pressure; the energy, which we can assume is equal for all atoms in the environment, and the number of atoms bombarding the surface, which is proportional to the number of atoms in the environment. In this way we can say that the less atoms there are in the environment, the lower the pressure and the longer the sample will remain useable. We could also reduce the temperature to reduce the pressure but to reduce it to the extent necessary ($3 * 10^{-11} K$) would be unfeasible.

UHV is of the order of 10^{-10} mbar which is incredible. The equipment used was less than $2m^3$ in volume so to show how good the vacuum is I will go through a quick calculation.

Number of molecules per m^3 at atmospheric pressure:

$$N_{atm} = 2.5 * 10^{25}$$

Number of molecules per m^3 at UHV:

$$N_{UHV} = 2.5 * 10^{12}$$

At UHV our system has an environment with roughly $2N_{UHV} = 5 * 10^{12}$ molecules so let's see how much volume would this take up at atmospheric pressure.

$$\frac{2N_{UHV}}{N_{atm}} = 2 * 10^{-13} m^3 = 0.0002 mm^3$$

This much air would fit under my little finger nail with a lot of room to spare. From this it can be seen that even the slightest leak would destroy a UHV environment.

5.2 Creating a Vacuum

As mentioned above, UHV is necessary to maintain a clean surface for enough time to perform an experiment. High vacuum, $10^{-6}mbar$, is just not good enough. At this pressure a monolayer will form in around 1 second. Getting down to UHV has been made relatively easy by the invention of the turbomolecular pump but “relatively easy” still takes around a day of preparation.

Rotary Vane Pump The rotary vane pump is a roughing pump which means it can only reach a rough vacuum of around 10^{-2} mbar. It is necessary because most UHV pumps won't work in atmospheric pressure for reasons I will go into later. This pump works by rotating a spring driven sliding vane inside a chamber in the pump. The pump is linked to the vacuum chamber on one side and has an exhaust at atmospheric pressure on the other. The vacuum system is always sealed off from the atmosphere. As the vane begins to rotate around the pump it increases the volume of the vacuum system. This decreases the pressure which can be seen in the ideal gas equation $PV = nRT$. At this stage the temperature and number of molecules are constant. When the vane has rotated 180 degrees it seals off the vacuum chamber. At this point the volume drops instantly back to its original value while the pressure remains at the lower value. The molecules inside the pump are forced out of the exhaust. Disadvantages to this design are the need for oil and condensation in the compression phase. Oil, or any hydrocarbons, are difficult to remove from vacuum equipment and molecules can make their way into the vacuum system. A Zeolite trap can be used to stop this though it is not needed when using a Turbomolecular pump for reasons I will go into later.

Turbomolecular Pump This was the main UHV pump we used in combination with the rotary vane roughing pump. It is commonly described as

a small jet engine. The aim of this pump is to give momentum to molecules that are in it, forcing them to move towards the roughing pump. It does this by repeatedly bashing them with angled rotors, aided by stationary stators which help direct the flow. This may not seem like an elegant solution but a UHV pump must maintain a pressure difference of 10^{-10} mbar at the vacuum system and 10^{-2} mbar which is the greatest vacuum a backing pump can manage. To redirect molecules effectly the rotors must be moving at a velocity which is comparable to the molecules' velocities therefore, the rotors must have a rotation of 90000rpm. To create a pump which can do this requires fine precision, as any fluctuation in the position of the rotors will cause a disastrous impact destroying the equipment and creating a lot of shrapnel. To remove the chance of this the bearings are usually an air or magnetic bearing as these do not wear down. As mentioned the rotors move at a comparable speed to the gas molecules, however heavier molecules move slower than lighter molecules and are therefore compressed at a greater ratio. Hydrocarbons are generally very heavy so, when a turbomolecular pump is used in conjunction with a rotary vane pump, any oil released is kept behind the turbomolecular pump. This removes the need for a Zeolite trap. The limitation for this method is the backing pressure. The disadvantage of this method is that it cannot be switched on when attempting to get atomic resolution in STM due to mechanical noise from vibrations.

Titanium Sublimation Pump (TSP) The TSP uses the chemisorption properties of a titanium film to catch molecules hitting it. It creates this film in a separate chamber bolted onto the vacuum system by passing a large current of 40 amps through a filament in the center, this is known as "firing". The filament is an alloy of Ti/Mo. Some of the Ti in the filament vapourises and moves away, it strikes the wall of the TSP chamber and binds forming a film. Any gas molecules which strike this film bind to it, reducing the number



Figure 11: Picture of a turbomolecular pump

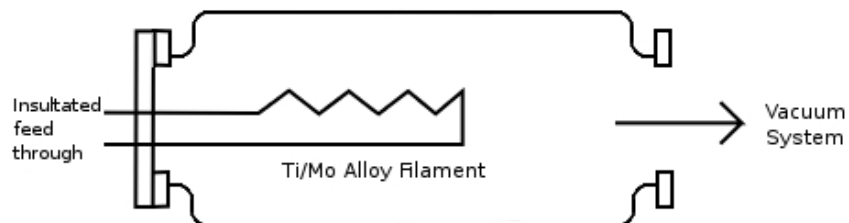


Figure 12: Schematic diagram of a TSP

of free molecules and thus the pressure. This can be repeated and the new layer of Ti “burys“ the layer of gas molecules. The main disadvantage of this method is that it can contaminate a sample if it is in the chamber when the TSP fires. It was used as an aid to reach low pressures faster before any sputtering or annealing took place.

Sputter Ion Pump The Sputter Ion pump works in a similar way to the TSP except that the Ti is ionised and there is a lot less of it. Two Ti cathodes are placed either side of an anode in the centre. With an electric field of 3 to 7 kV the Ti ionises and sputters away from the cathode. A magnetic field of 0.1 to 0.2 Tesla is also applied which causes the moving ions to spiral, therefore increasing the volume that the ions are travelling in. The Ti ions

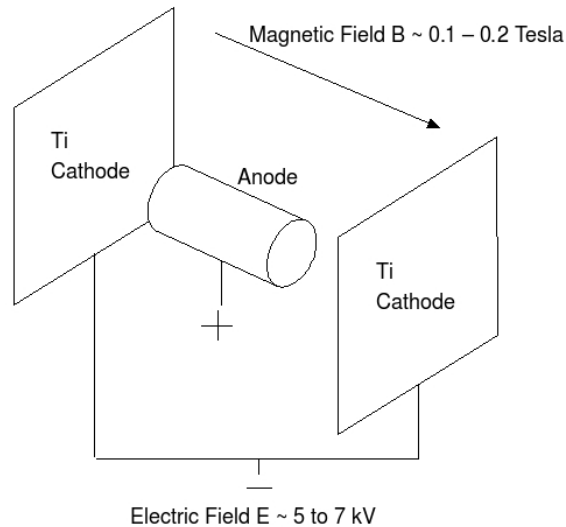


Figure 13: Schematic diagram of a Sputter Ion Pump

will bind to gas molecules and then stick to the anode, effectively burying them. When the Ti ions bind to the anode they form a film like the TSP, gas molecules hitting this film are bound by chemisorption. The disadvantage of this technique is it needs a pressure of less than 10^{-3} torr to operate. Operating at higher than this will cause a large current which in turn causes outgassing from the Ti film. The accompanied pressure increase causes the current to raise and thus more outgassing. This continues until a current cut off threshold when the pump trips off. We used this pump to maintain the required pressure during the STM runs as it is noiseless and does not contaminate the sample.

Venting Venting is the practice of the UHV chamber up to atmospheric pressure with nitrogen. This allows the experimenter to open the chamber without letting more oxygen and water vapour in than is necessary. Nitrogen is much more inert than either of these and the chamber can be brought to

UHV more quickly afterwards.

Baking Any exposure to the atmosphere will cause molecules to bind to the surface. These molecules will start to outgas as the chamber is evacuated and stop it from reaching UHV. If the chamber is pumped then it will eventually reach UHV, however this takes a long time so instead the equipment is heated. By heating the outgassing process is accelerated and the equipment is sufficiently degassed in a few hours.

5.3 LEED

In this project Low Energy Electron Diffraction or LEED was used to compare the sample to a better known material and thus gather some information about the structure. To explain LEED properly, the idea of the De Broglie wavelength must be briefly discussed. All particles can be assigned a wavelength (λ) which is dependent on their momentum (p), as shown in the following equation:

$$p = \frac{2\pi\hbar}{\lambda} \quad (1)$$

This can be seen in diffraction experiments, particles will behave the same as light with the same wavelength. For most energy ranges, the wavelengths of particles are much higher than the corresponding wavelength for light. This is due to the particles having mass.

Bragg Diffraction The easiest example of Bragg Diffraction is a 2D cross section of a grating with two rays of light entering from the left. These rays of light hit adjacent gaps in the grating. A wave passing through a gap of equal size to the wavelength of the wave will propagate in all directions on

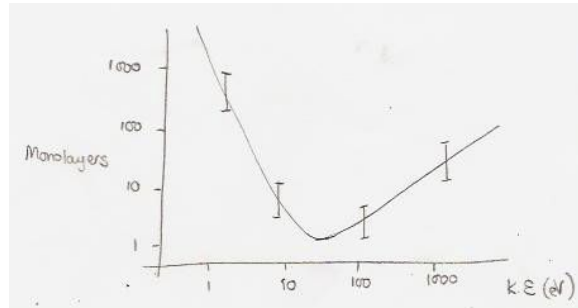


Figure 14: Graph describing Electron Energy vs Escape Depth

the other side. If the grating width is comparable to the wavelength of the light, the two incident rays will diffract. Depending on the angle in relation to the grating the light will interfere either constructively or destructively. Thus it can be seen that when a beam light is shone on a grating, bright spots are observed at certain angles (θ). These bright spots, or Bragg Peaks, can be found from the following formula:

$$2d \sin \theta = n\lambda \quad (2)$$

In the case of a 3D crystal, or quasicrystal, it is not a grating that causes the diffraction but the planes of the atom. Further to this, in the case of LEED it is not light which is used but low energy electrons.

Electron Energies vs Escape Depth It is possible to tune the beam energies so that the electrons escape at set depths. The following graph shows a universal curve which works in most cases with large error bars.

It can be seen that if the energy is set to 10-100 eV the electrons will only diffract off the top 1 or 2 monolayers, thus giving us information about

the surface.

LEED Patterns The set of bright spots produced during a LEED experiment is called a LEED pattern and is a representation of the 2D reciprocal lattice, averaged over all the atomic layers the electrons have escaped from. The reciprocal lattice of a real space lattice can be found with a matrix conversion.

5.4 STM

Scanning Tunnelling Microscopy is a relatively new way of imaging a surface. It can achieve atomic resolution on conducting or semi-conducting surfaces. Its limitations are the sharpness of the tip and that it measures electron density not the actual surface. An example of when electron density does not give a true image of the surface would be a Si (100) surface where free bonds of neighbouring atoms form dimers. These dimers will shown by the STM to be a single object, not a pair. In this case a true representation can be found by reversing the STM bias.

STM Operation The STM uses quantum tunnelling of electrons to detect changes in the height of the surface on the atomic scale. An electric potential (V) is set up between the tip and the sample; as the system is evacuated there is nothing to carry the current across the gap. Due to quantum mechanics the electron's wavefunctions have a probability distribution and they can effectively move from the tip to the surface, or vice versa, without needing material in the intervening space. This tunnelling produces a measurable current (I). The tunnelling current decays exponentially with distance (d) described by the equation:

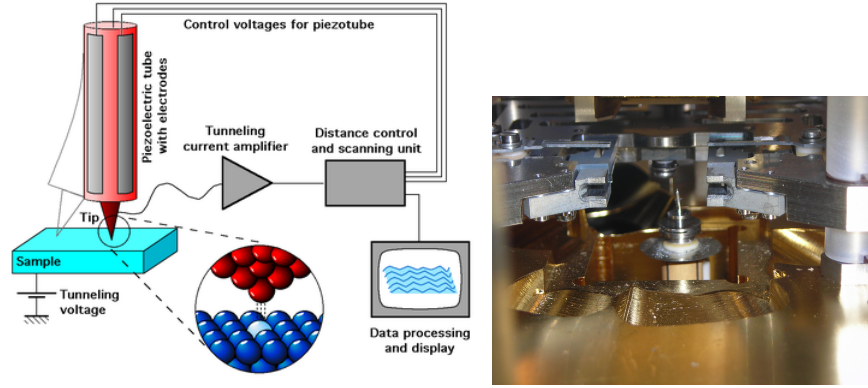


Figure 15: Left: Schematic diagram of an STM. Right: Picture of an STM tip in an STM machine

$$I \propto \left(\frac{V}{d}\right)e^{-\alpha d} \quad (3)$$

Where $2\alpha[\text{\AA}^{-1}] = 1.025(\phi[eV])^{1/2}$

and ϕ is the work function of the surface and the tip

5.5 Ion Sputtering

When a sample is polished in air at atmospheric pressure, the clean surface reacts to form an oxide almost instantly (need some workings here). It is therefore necessary to do some sample preparation in the chamber. When the chamber is at UHV it is sealed off and argon is released to bring the pressure up to 10^{-6} mbars. Argon is a noble gas, and therefore inert, so it does not react with the surface. Before this some of the argon is released to make sure that the argon used is clean. The Argon is ionised and then accelerated towards the sample using an electric field where it impacts at high speed. This causes a few sample atoms to become detached and move

away from the surface. The argon ion deionises and bounces away. The beam of argon ions can be likened to a very fine abrasive, as it wears down the surface very slowly.

5.6 Annealling

After sputtering, the surface is too rough for STM. The composition of the surface after STM may also be different to its normal surface. To restore the surface to its natural state we must anneal. This is the process of heating the sample and giving the atoms kinetic energies. The extra energy allows them to overcome potential barriers and rearrange into their lowest energy states. This restores the most stable surface which in the case of our AgYbIn quasicrystal was the 5 fold symmetry surface.

5.7 Diamond Paste Polishing

Sputtering and annealing does little of use if the sample has not been polished to start with. We used a combination of abrasive paper and diamond paste of different grades. This was followed by a ultrasound bath in methane to clean any diamond left after polishing.

6 Experiments

6.1 Step Morphology

As with the fivefold surface of Al based quasicrystals, the Ag based crystal also showed very rough step edges for the most part. In some places on the surface the steps did tend to form a long, almost straight, line. I believe that some terraces are more prone to this than others.

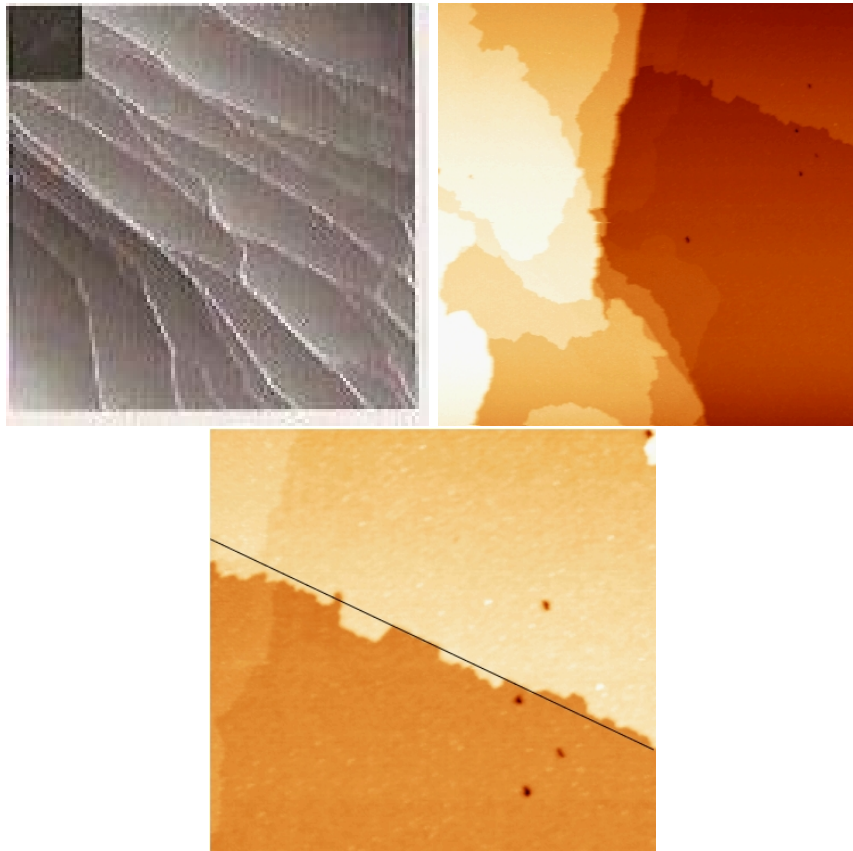


Figure 16: Top Left: *i*-Al-Pd-Mn $700 \times 700 \text{nm}^2$, shows slight curve in all step edges. Top Right: *i*-Ag-Yb-In $500 \times 500 \text{nm}^2$, Shows straighter edges in parts. Bottom: *i*-Ag-Yb-In $250 \times 240 \text{nm}^2$, line has been drawn to show how the step would be if it were straight.

The angles between the deviations are 108° which is related to the fivefold symmetry. The gaps between the deviations form a fibonacci sequence of small and large gaps.

A screw dislocation was seen on the surface, it must be assumed they are rare as no more were found.

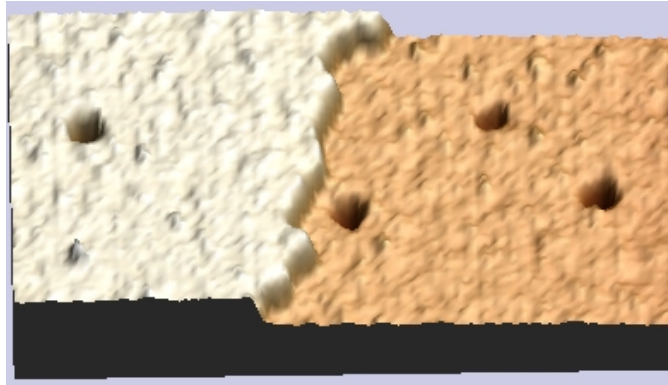


Figure 17: *i*-Ag-Yb-In surface 60nmx135nm, shows pits in surface

6.2 Terrace Morphology

Terrace size was a big problem for us as it varies with preparation and the best preparation for the fivefold plane of *i*-Ag-Yb-In has not been established yet. The quasicrystal also had two different quasicrystal domains and a periodic domain which will all be discussed in more detail later. The fivefold axis for one of the domains was not perpendicular to the surface, leading to many small terraces. This is because the fivefold surface is the least energetic and is preferred. In the domains with small terraces they were less than 100 nm wide. In domains where the fivefold axis was perpendicular to the surface there were terraces greater than 500nm wide.

Small pits were found on the surface, they are around 7.5nm in diameter and have a depth of one monolayer.

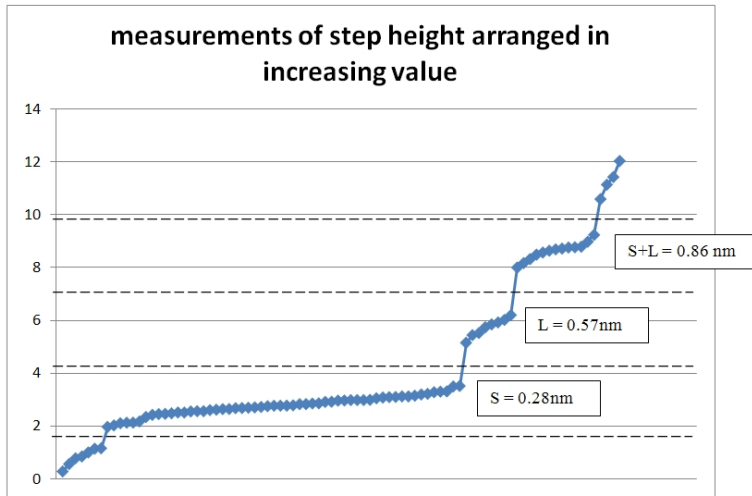


Figure 18: This graph shows all of the step height measurements taken and arranged in height order. It shows the step heights as jumps in the step height.

6.3 Step Height Distribution

As the *i*-Ag-Yb-In sample is quasicrystalline in 3 dimensions it should have non uniform step heights. By measuring these it can be found that there are three different heights which have been labelled S, L and S+L. By taking measurements of different steps using STM a statistical distribution with errors can be produced. The following data was produced from 88 different steps.

S $\rightarrow 0.28 \pm 0.04\text{nm}$; probability = $64 \pm 8\%$

L $\rightarrow 0.57 \pm 0.03\text{nm}$; probability = $9 \pm 3\%$

S+L $\rightarrow 0.86 \pm 0.03\text{nm}$; probability = $15 \pm 4\%$

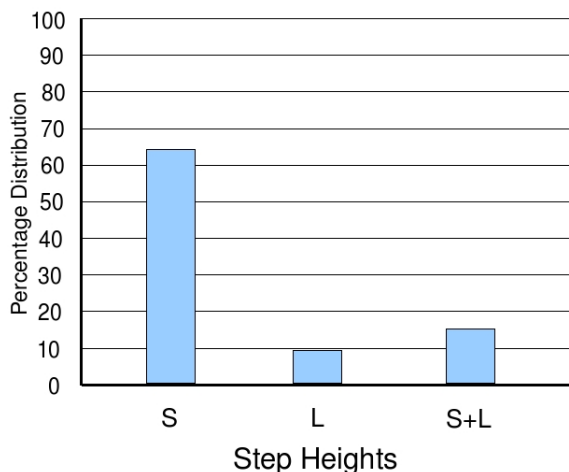


Figure 19: This is a graph showing the percentage distribution of step height.

6.4 High Resolution Image

The most interesting data came from the STM images. It took many attempts to get a large terrace but in the end we managed to get some very good results. The best of the data taken until that point looked like this:

The terraces like the ones to the top left are common across the surface. The larger flat terraces were rare and still too small to properly experiment on. With image analysis tools I zoomed in on the terrace and then looked at the FFT (What is this?).

There are 10 clearly defined dots in the FFT which map out a circle. These are from parts of the image which show 5-fold rotational symmetry. Using the analysis tools I filtered out all the noise and merged this new image with the original to highlight these parts of the image.

The resulting image is a little better and with a bit of imagination it is possible to see pentagons but the quality is still too poor to determine any-

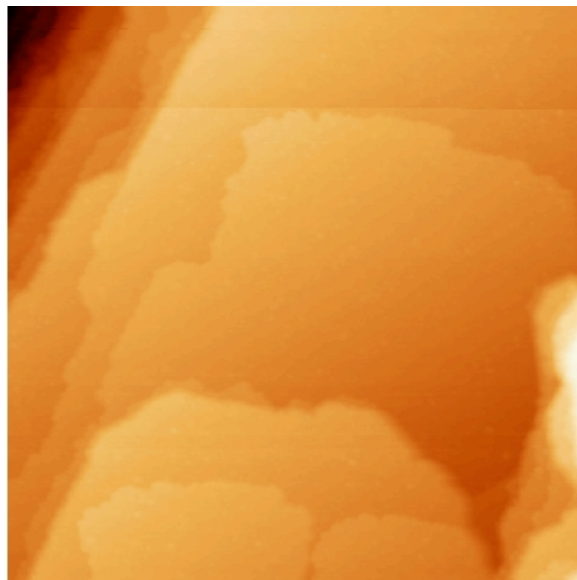


Figure 20: *i*-Ag-Yb-In, 5-fold surface 200nm x 200nm.

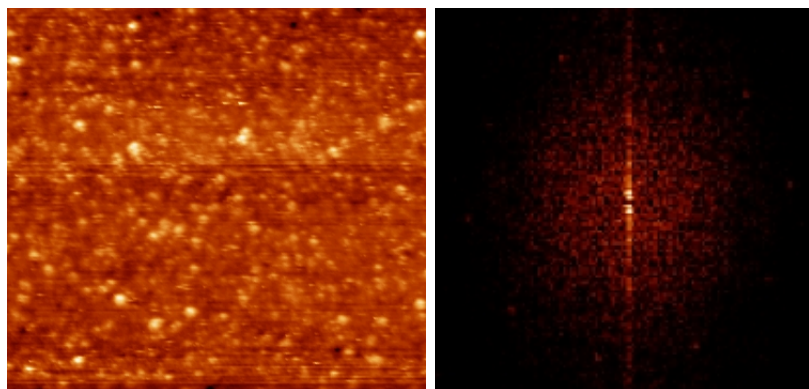


Figure 21: Left: Zoomed in section of the large terrace 84nm x 77.3nm.
Right: FFT of terrace, shows faint fivefold symmetry

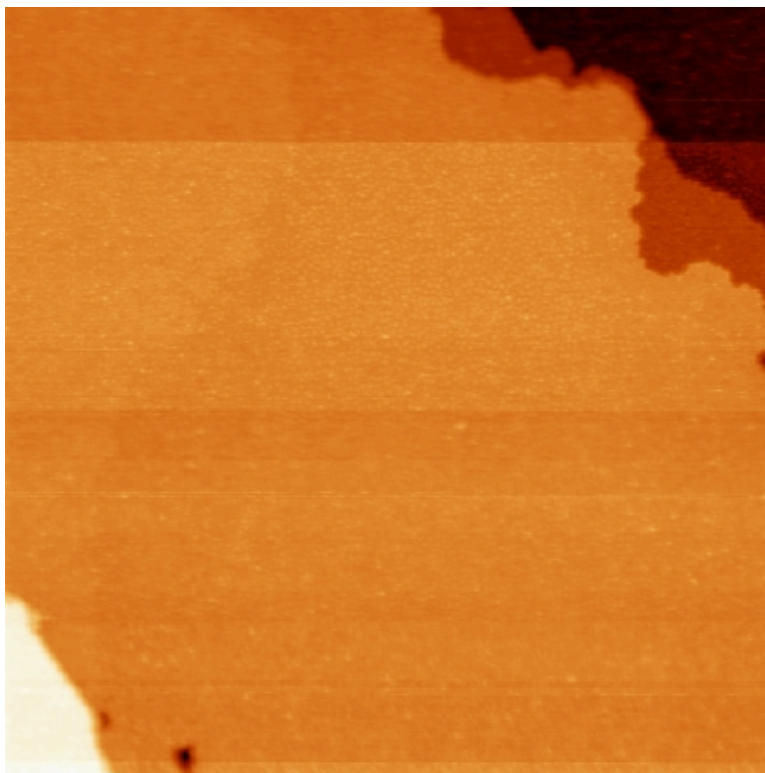


Figure 22: 257x257nm *i*-Ag-Yb-In surface

thing useful. It is not possible to conclude that the surface is quasicrystalline without a higher resolution image; this requires a larger flat terrace. Luckily we found an area on the surface a couple of days later where the terraces were larger than any we had seen previously.

Even at this scale the resolution was high enough to make out clusters but when we went down to 50x50nm they became very easy to see.

From here I could again filter the image and merge with the original to improve the quality. By zooming in on this new image it is easy to see the individual clusters.

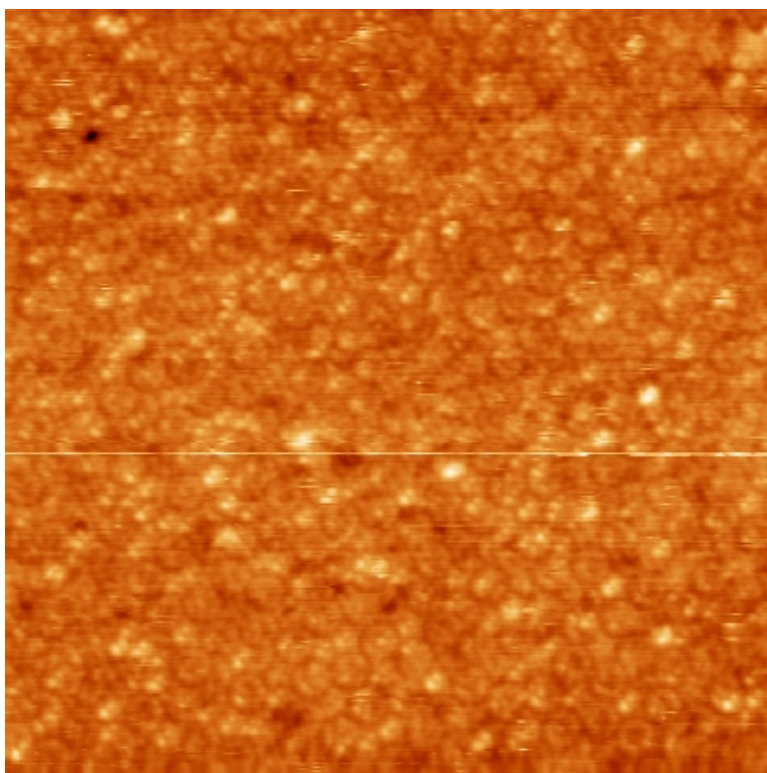


Figure 23: *i*-Ag-Yb-In 50x50 nm² high resolution unedited image

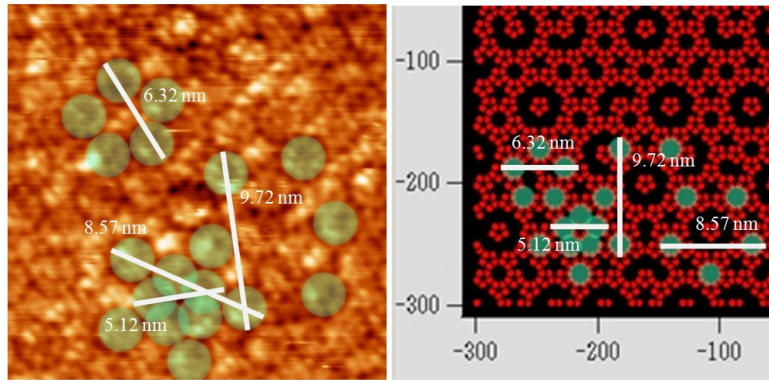


Figure 24: Left: *i*-Ag-Yb-In 50x50 nm² filtered. Right: Modal of a Yb surface, equivalent measurements marked on each image

With the high resolution image I went on to compare this new image with a modal. The red dots in the modal are Yb sites and simulate the structure of the Yb in a *i*-Cd-Yb binary quasicrystal. Only Yb is simulated because it has the lowest surface energy and is more likely to form a stable surface. As the *i*-Ag-Yb-In quasicrystal is meant to be of the same structure as *i*-Cd-Yb then the modal should be able to work for my sample too.

In the STM image decagons of dark spots can be seen. If compared to the modal image decagons of light spots can be seen. Both of these are highlighted, however on closer inspection we can see the decagons in the modal are made from very small pentagons. These pentagons have a gap in the middle of them and gaps between them. The gaps make a decagon of the correct size when compared to the real image. This the dark decagon on the real image and circle of points below both have a diameter of 2.84nm.

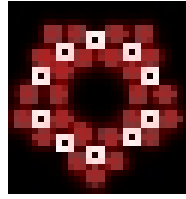


Figure 25: Model of a cluster of Yb atoms, the highlighted dark spots are seen in the real image.

6.5 LEED - Long Range Order

Using LEED we scanned the *i*-Ag-Yb-In quasicrystal to see if it had long range order and to find its rotational symmetry. After this, by comparing the LEED pattern with a LEED pattern for a quasicrystal we know the lattice vector for, it is possible to work out the lattice vector of *i*-Ag-Yb-In with the ratio. The LEED must be set to the same energy for this and the patterns below were both created with a beam energy of 35.6 eV with the same LEED machine and set up.

The image from the *i*-Ag-Yb-In shows a pentagon, this confirmed that it has long range order and fivefold symmetry. As the magnitude of the reciprocal lattice vectors for *i*-Al-Pd-Mg is 0.99 \AA^{-1} [3] and the ratio between the sizes of pentagons is 0.51 I can say that the lattice vectors for AgTbIn should be around 0.51 \AA^{-1} .

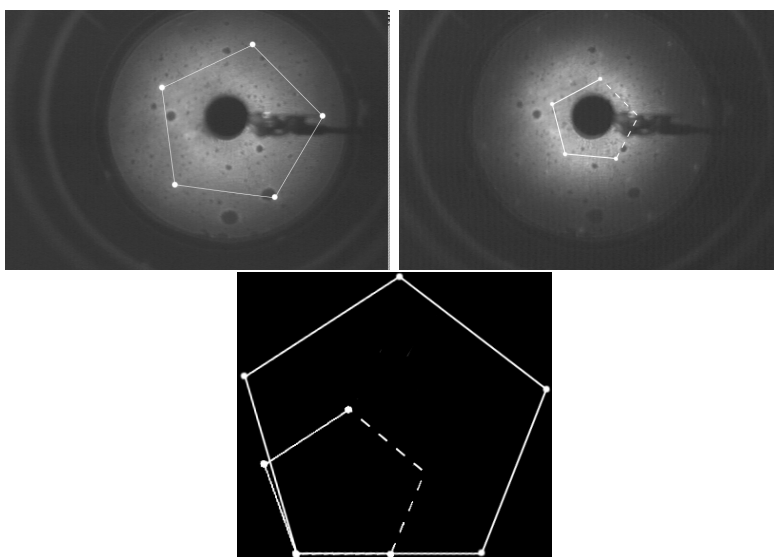


Figure 26: Top left: *i*-Ag-Yb-In quasicrystal LEED pattern. Top Right: *i*-Al-Pd-Mg quasicrystal LEED pattern. Bottom: Comparison of the two Pentagons In the different LEED patterns.

6.6 Different Domains in the Sample

When experimenting on our sample we found it has a few different domains. Domains are not good for the experiments we wished to perform. Ideally the best sample would have been one with the fivefold axis perfectly perpendicular to the surface, however this was not the case. There were at least two quasicrystalline domains oriented differently to each other. The inclination between these two domains could be measured using LEED but that was not within the scope of this project. The oddest thing about the sample is that part of it is actually periodic when seen with a LEED pattern.

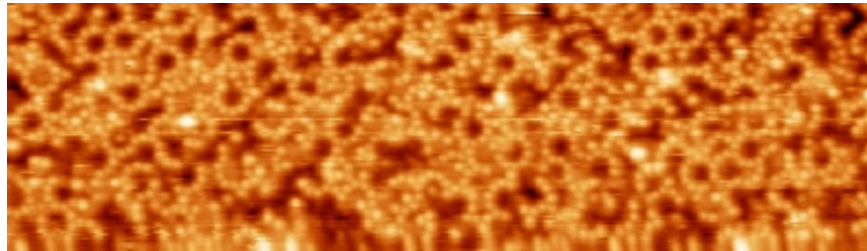


Figure 27: STM image *i*-Ag-Yb-In 76.8x22nm one lead monolayer deposition

6.7 Pb and C60 Deposition

Using an evaporator we deposited lead onto the clean surface. From the image it can be seen that lead forms a quasicrystalline monolayer. This is seen in the form of decagons. The lead atoms are much larger than the atoms in the quasicrystal therefore they are much easier to see and make an impressive STM image. Comparing the size of the lead decagons to the high resolution image it can be seen that they are the exactly the same size as the dark decagons. I would guess that the lead atoms are sticking in the gaps in the quasicrystal but this lies outside the scope of this project.

Following on from this we deposited C60 but found that little of interest happened. The size of the C60 can be seen here though it does show how big lead atoms are. The white blobs are sixty carbon atoms and yet the individual lead atoms are still visible.

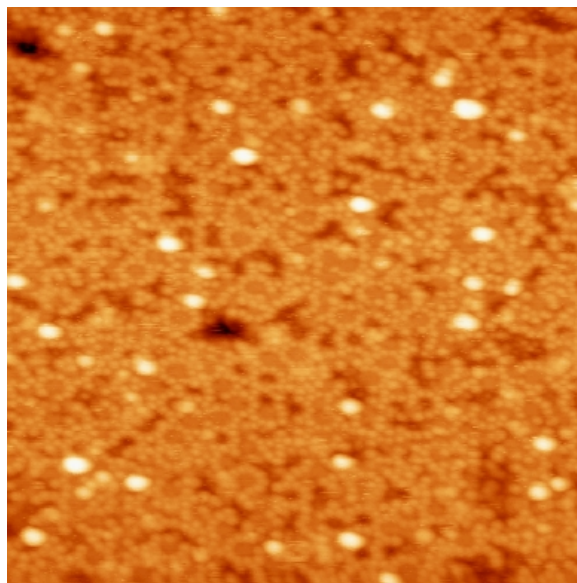


Figure 28: STM image *i*-Ag-Yb-In one lead monolayer deposition followed by C60 deposition

7 Conclusion

Using STM and LEED in a UHV system we attempted to make some progress in the characterisation of the *i*-Ag-Yb-In quasicrystal.

My first task was to try and look into step and terrace morphology. I found that the step edges on some terraces were straighter than others. The defects from a straight line in the steps were always at an angle of 108 degrees; confirming the pentagon based structure of the surface. We found screw dislocations on the surface at an annealing temperature of 435 C. The terraces sizes were in excess of 500nm and I would expect to find larger ones on a better sample. Small pits were found in the sample with a diameter of 7.5nm and a depth of one monolayer.

Secondly I looked at the step height distribution and found three distinct step heights. The probability distributions for these steps was found to be $S \rightarrow 0.28 \pm 0.04\text{nm}$; probability = $64 \pm 8\%$; $L \rightarrow 0.57 \pm 0.03\text{nm}$; probability = $9 \pm 3\%$ and $S+L \rightarrow 0.86 \pm 0.03\text{nm}$; probability = $15 \pm 4\%$.

Thirdly I analysed a high resolution image of the surface and compared it to a model of Yb atom placements generated by **. The match I found had similar features and the sizes were correct also.

Fourthly I looked at LEED patterns of the sample. In doing so I proved the sample was fivefold symmetric. By comparing it to LEED patterns of *i*-Al-Pd-Mn taken under the same conditions, I found the ratio of the magnitudes of the lattice vector. Using the ratio and the already known lattice vector magnitude of $.99 \text{ \AA}^{-1}$ for *i*-Al-Pd-Mn, I estimate the lattice vector magnitude for *i*-Ag-Yb-In to be 0.51 \AA^{-1} .

During our experiments it was noticed that the sample was not a single grain quasicrystal like we thought; it had different domains. Using LEED we found at least two differently orientated fivefold domains and a periodic domain. Finally we successfully deposited a monolayer of lead on the sample surface and took high resolution STM images. We followed this with the deposition of C60 which destroyed the fivefold symmetry.

I think most of all I enjoyed working with other people who are more knowledgeable about the project than me. If I ever had a question I could just ask and it would be explained to me. I found it much easier to learn like this than attempting to learn from a book or notes. I also enjoyed the analysis, making my way through the data was tedious but when I finally came to something new it was very interesting.

I found the experiments very challenging. It wasn't that they were very difficult; it was the having to start from the beginning if something went wrong. I did not find anything unlikeable but I could imagine it can get a bit frustrating if it happens all the time.

There is great potential for future work stemming from the material covered in this project. The composition of the different terraces could be looked at, to see if I was correct in my assumption that the terraces have different surface energy. From this we could find the composition of the most stable surface. With respect to the sample we could go on to investigate the different domains; possibly allowing us to understand how they formed and prevent it from happening in future. Finally the most important future work would be depositing thin films on the surface. There are many possibilities to explore and to the combination of surface and coating, perhaps one will extend more than a monolayer and solve the quasicrystal production problem.

References

- [1] C. Janot: *Quasicrystals A Primer*, second edition, Oxford Science Publications (1999), editors: R. J. Brook, T. Cheetham, A. Heuer, P.B. Hirsch, T.J. Marks, D.G. Pettifor, M. Ruhle, J. Silcox, M. Tirrel, V. Vitex
- [2] E. Abe, K. Saitoh, H. Takakura, A.P. Tsai, P.J. Steinhardt, and H.-C. Jeong, Phys. Rev. Lett. 84, 4609 (2000).
- [3] H.R. Sharma, M. Shaimoda, A.P. Tsai: *Quasicrystal surfaces: structure and growth of atomic overlays*, Advances in Physics, Volume 56, Nos. 3-4, Pages 403-464, (2007)
- [4] <http://www.dvorsons.com/Sitram/Cybernox/Cybernox.html>
- [5] A.P. Tsai and M. Yoshimura, Appl. Catal. A-Gen **214** 237 (2001)
- [6] Joseph A. Smerdon: *The formation and characterisation of aperiodic ultra-thin films on the surfaces of quasicrystals*, PhD Thesis, University of Liverpool, (2006)
- [7] D. Shechtman, I. Blech, D. Gratias, and J.W. Cahn, Phys. Rev. Lett **53**, 1951 (1984).
- [8] P. Guyot, P. Kramer, and M. de Boissieu, Rep. Prog. Phys. **54**, 1373 (1991).
- [9] J.Q. Guo, T.J. Sato, E. Abe, H. Takakura and A.P. Tsai, Phil. Mag. Lett. **88** 495 (2000)
- [10] A.P. Tsai, Acc. Chem. Res. **46** 31 (2003)